Electronic supplementary information for

In-situ probing of the interfacial kinetics for studying the electrochemical properties of active particles and the state of health of Li-ion batteries

Wenju Ren, Haibiao Chen, Rongxue Qiao, Yuan Lin*, and Feng Pan*

School of Advanced Materials, Peking University, Shenzhen Graduate School,

Shenzhen, 518055, People's Republic of China.

*Corresponding Authors

E-mail: panfeng@pkusz.edu.cn (FP), linyuan@iccas.ac.cn (YL)

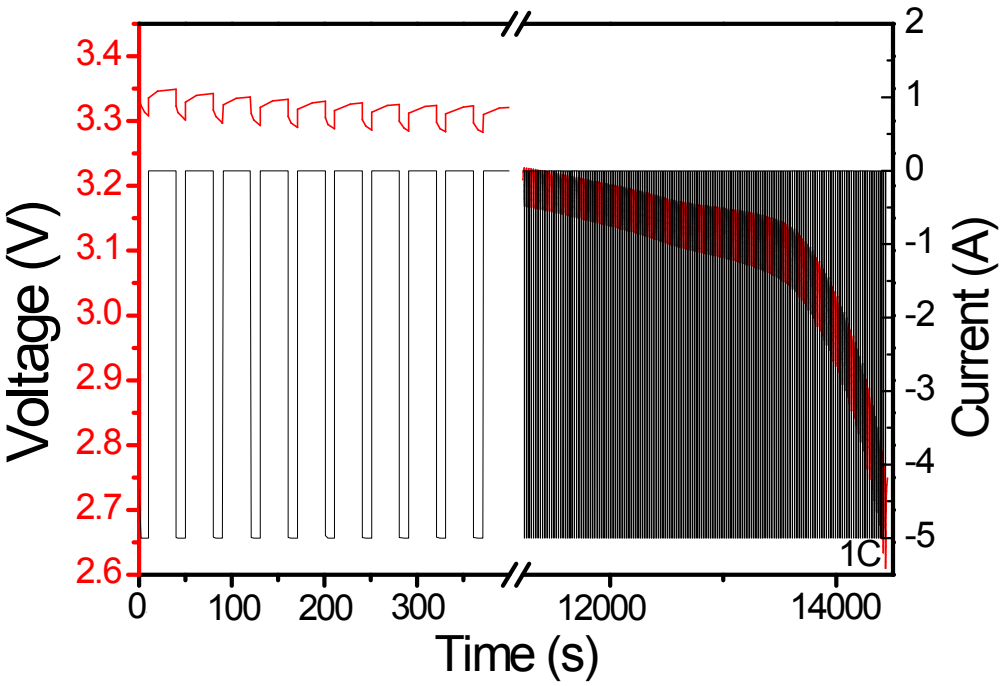

Fig. S1 Current and voltage curves during discharge

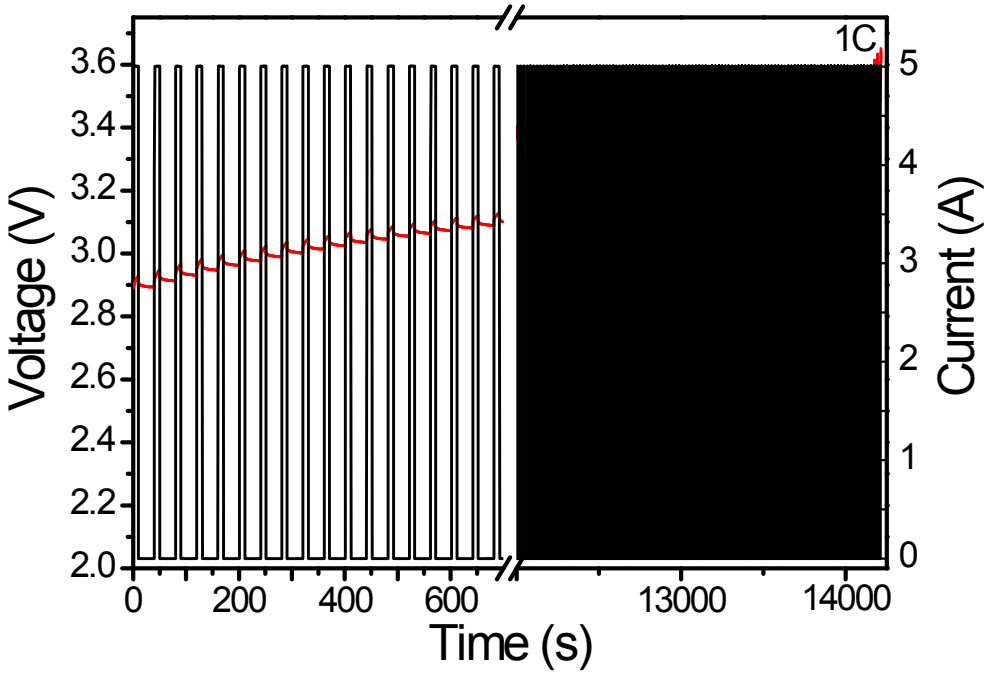

Fig. S2 Current and voltage curves during charge

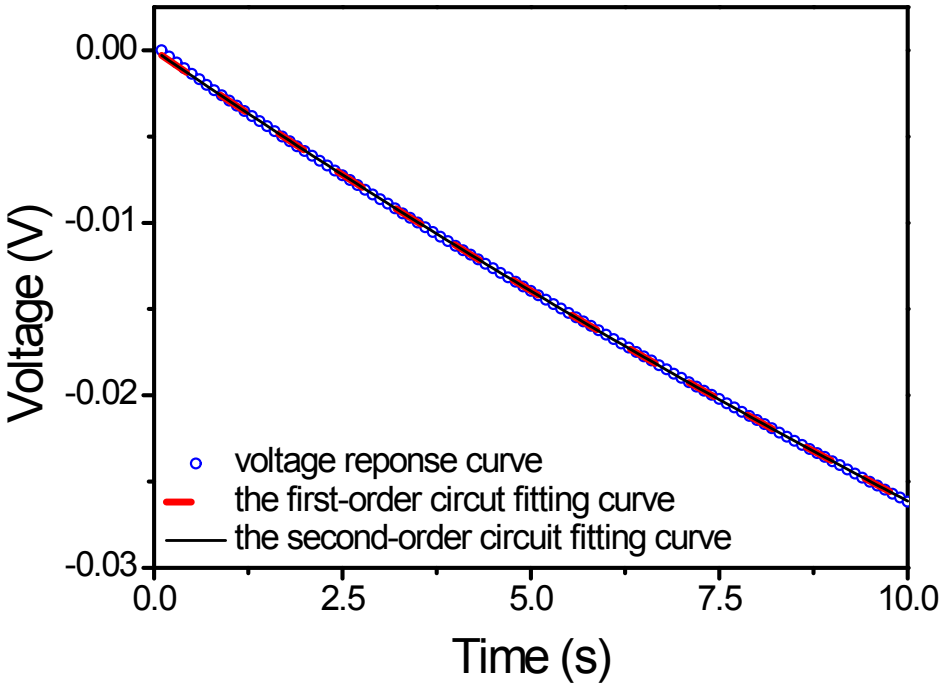

Fig. S3 Voltage response curve and fitting

Table S1 The first-order RC circuit fitting results

Reduced Chi-Sqr	2.95984E-9
Adj. R-Square	0.99995
Parameters	Value
R_p	0.010248 Ω
C_p	605.786 F

Table S2 The second-order RC circuit fitting results

Reduced Chi-Sqr	3.02151E-9
Adj. R-Square	0.99995
	Value
R_{p1}	0.001712 Ω
C_{p1}	233.6449 F
R_{p2}	0.01876 Ω
C_{p2}	21.322 F

S1. Battery disassembly procedure

In this work, to disassemble the cylindrical cell, a diagonal cutting nipper and a pipe cutter were used.

Fig. S4 The diagonal cutting nipper, pipe cutter and battery.

First, the cell was cut along the peripheral groove using pipe cutter.

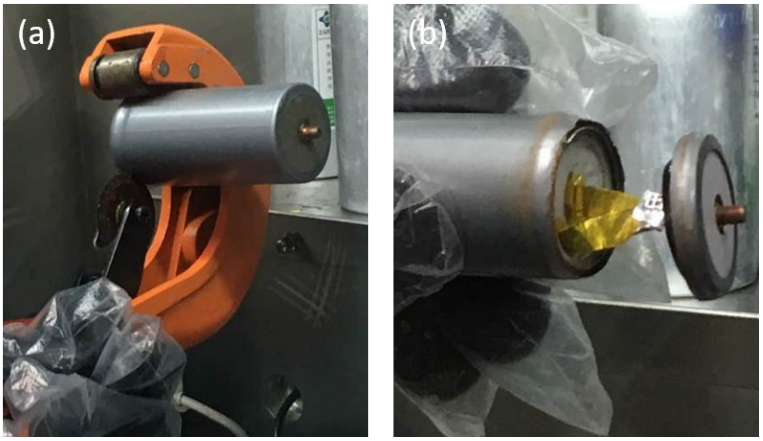

Fig. S5 (a) During cutting and (b) after cutting.

Second, the upper cover and the steel shell were removed carefully, and the cathodic current-collector was cut using the diagonal cutting nipper to prevent short circuiting.

Fig. S6 After removing the upper cover and the steel shell.

Third, the steel shell was removed using the diagonal cutting nipper carefully.

Fig. S7 Removing the steel shell.

At last, the anode current-collector was cut from the steel shell.

Fig. S8 The roll from the battery

The anode and cathode were separately removed from the roll.

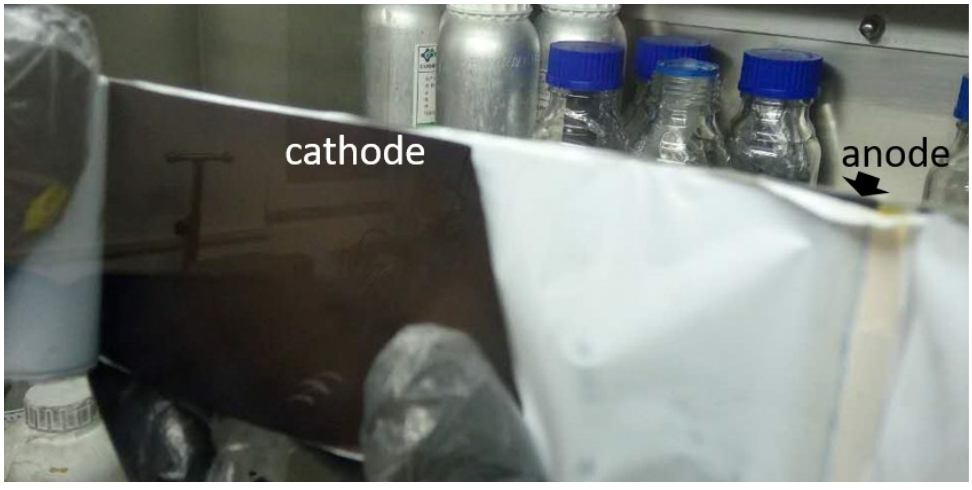

Fig. S9 The cathode, separator and anode.

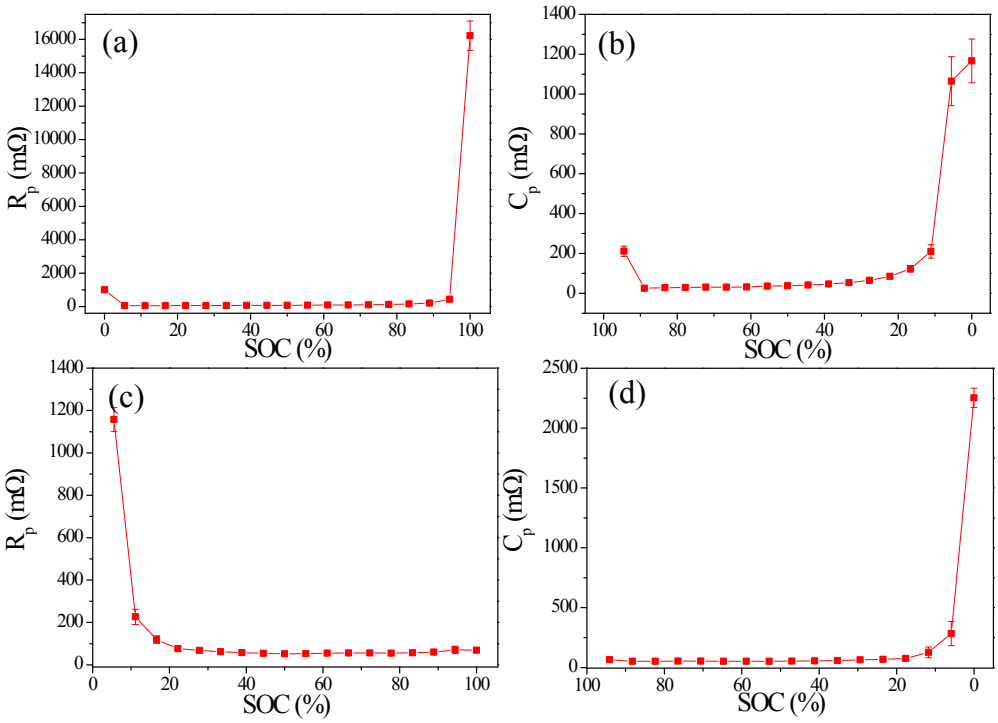

Fig. S10 The R_p curves of new LFP half-cells during (a) charge (b) discharge; the R_p curves of new graphite half-cells during (c) charge (d) discharge.

S2. Calculation of EDLC

The electrical double-layer capacitance (EDLC) can be deduced using the following method. First, the total available surface area per square meter of electrode surface can be derived use Eq. (S1):

$$S = {}^{V}\!/_{V_p} \cdot S_P = \left({}^{H \cdot l \cdot l}\!/_{4\pi \cdot r^3/3} \right) \cdot 4\pi r^2 = 450\ m^2 \quad \text{(S1)}$$

We assumed that the LFP particles were spherical as shown in **Figure S9**, and in Eq. (S1) V is the volume of the electrode per square meter, V_P is the average volume of the LFP particles, S_P is the average surface area of the LFP particles, r is the average radius (approximately 200 nm) of the LFP particles, H is the electrode thickness which was about 30 μm as shown in **Figure S6**, and l is the unit length which is one meter. Using Eq. (S1) we can deduce the total available surface area per m^2 of the electrode surface is 450 m^2.

Assuming the area-normalized specific capacitance is 20 mF/cm^2, [1-3] we can deduce the typical electrical double-layer capacitance (EDLC) of the electrode in 2032-type half-cells following equation:

$$C_{EDLC} = \pi \cdot R^2 \cdot S \cdot 20\ \mu F/cm^2 = 0.0025\ F \quad \text{(S2)}$$

where R = 3 mm is the electrode radius, S is total available surface area per square meter electrode surface, which is 450 m^2. Apparently the capacitance derived in the battery health model was far greater than EDLC. Therefore the C_p values were not solely contributed by the double layer capacitance. The diffusion and migration of the Li-ions in electrode and electrolyte should be the principal contribution to the capacitance in the battery health model.

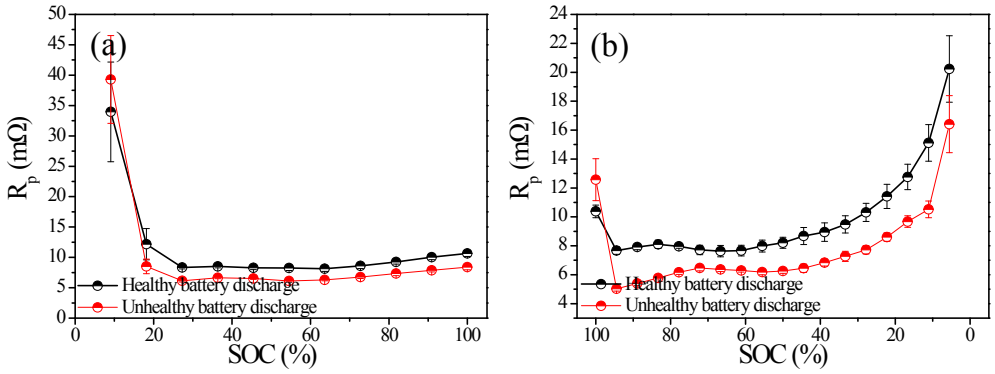

Fig. S11 The R_p curves of the healthy and unhealthy batteries during (a) charge and (b) discharge.

S3. The impedance measurement and fitting

To analyze the capacitance value of equivalent circuit of this battery, electrochemical impedance (EIS) measurements were carried out at various states of charge (SOC=50%) using a Solartron 1470E controlled by 1400A. The frequency spectrum for this work was limited to frequencies in the range of 10 kHz to 10 mHz, operating in galvanostatic mode with a signal amplitude of 10 mA and dc current 0 A. Impedance measurements were taken after a 6 h stabilization period at 25°C.

The equivalent electrical circuit model used to fit the impedance of Li-ion battery is shown in **Fig. S12**.

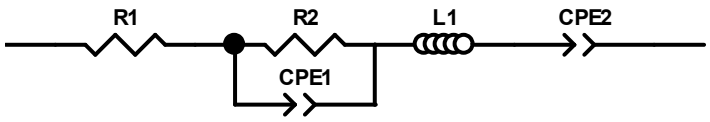

Fig. S12 Equivalent electrical circuit model

The model consists of five components. The first one is a resistance (R1) used to model the global ohmic behavior of the battery including metallic connection, electrode material and the bulk electrolyte. This model includes also an inductance (L) for modeling the inductive behavior of windings, a resistance (R2) in parallel with a constant phase element (CPE2) for modeling the charge transfer and double-layer processes.

The fitting results are shown in **Fig. S13** and **Table S3**. Because the diffusion of species dominates at low frequencies, it can be modeled by a Warburg element. In the fitting results we can find that the EDLC is only about 3.972F.

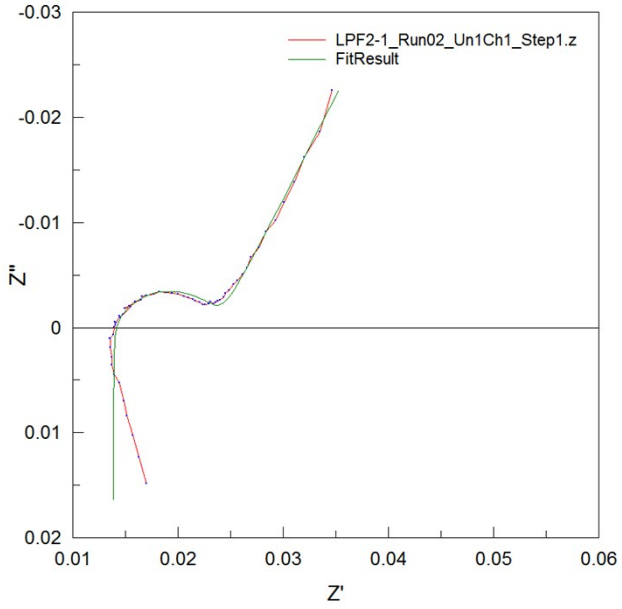

Fig. S13 Comparison of measured and simulated spectra of LFP/graphite battery

Table S3 The fitting results

Element	Freedom	Value	Error	Error (%)
R1	Fixed	0.013858	N/A	N/A
R2	Fixed	0.010012	N/A	N/A
CPE1-T	Fixed	3.972	N/A	N/A
CPE1-P	Fixed	0.74138	N/A	N/A
L1	Free	2.6111E-7	4.9091E-9	1.8801
CPE2-T	Free	274	8.0854	2.9509
CPE2-P	Free	0.69962	0.011191	1.5996
Chi-squared	0.0055989			
Weighted sum of squares	0.66627			

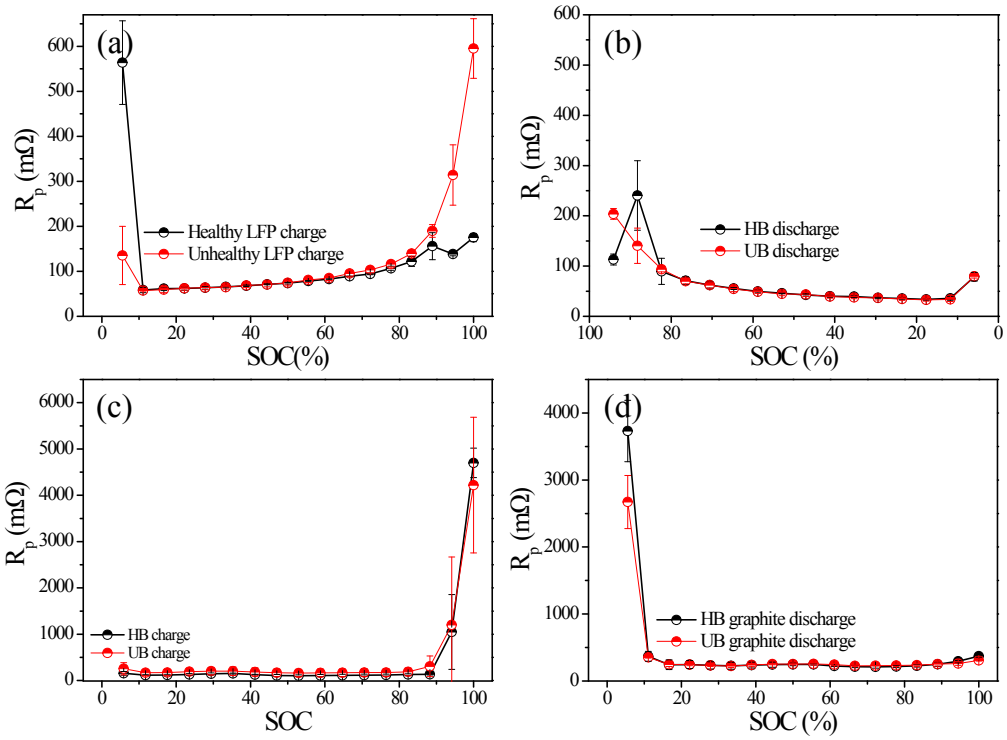

Fig. S14 The R_p curves of LFP half-cell made from healthy and unhealthy LFP electrodes during (a) charge and (b) discharge; the C_p curves of graphite half-cell made from healthy and unhealthy graphite electrode during (c) charge and (d) discharge.

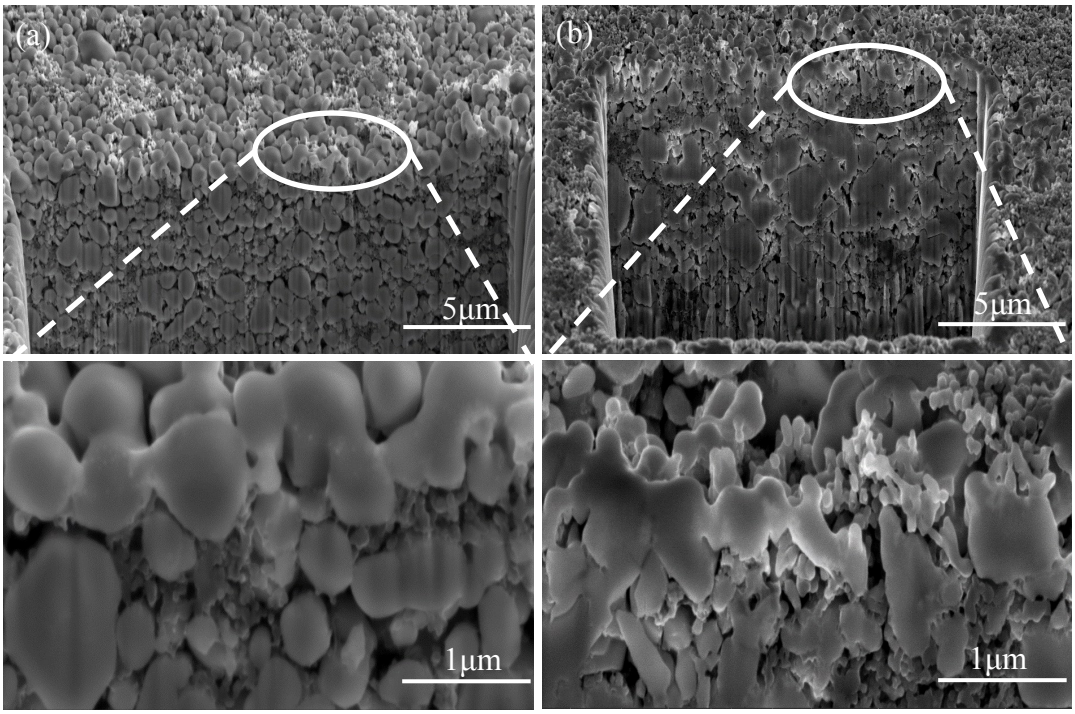

Fig. S15 SEM images of (a) healthy (b) unhealthy LFP electrodes.

Table S4 The R_a of healthy and unhealthy $LiFePO_4$ electrodes from batteries

Electrode	**R_a (mm)**
Healthy cathode	1.6589
Unhealthy cathode	2.3614
Healthy anode	2.4621
Unhealthy anode	4.5503

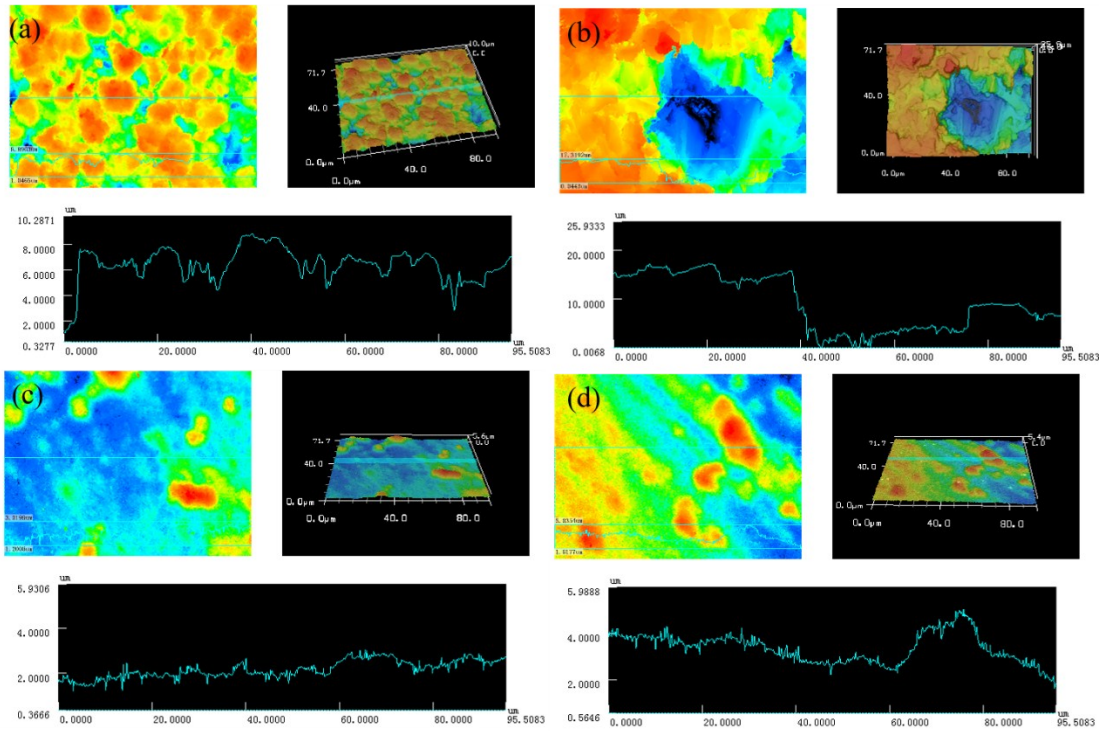

Fig. S16 3D laser confocal images of electrode surface (a) the healthy battery's anode, (b) the unhealthy battery's anode, (c) the healthy battery's cathode, (d) the unhealthy battery's cathode

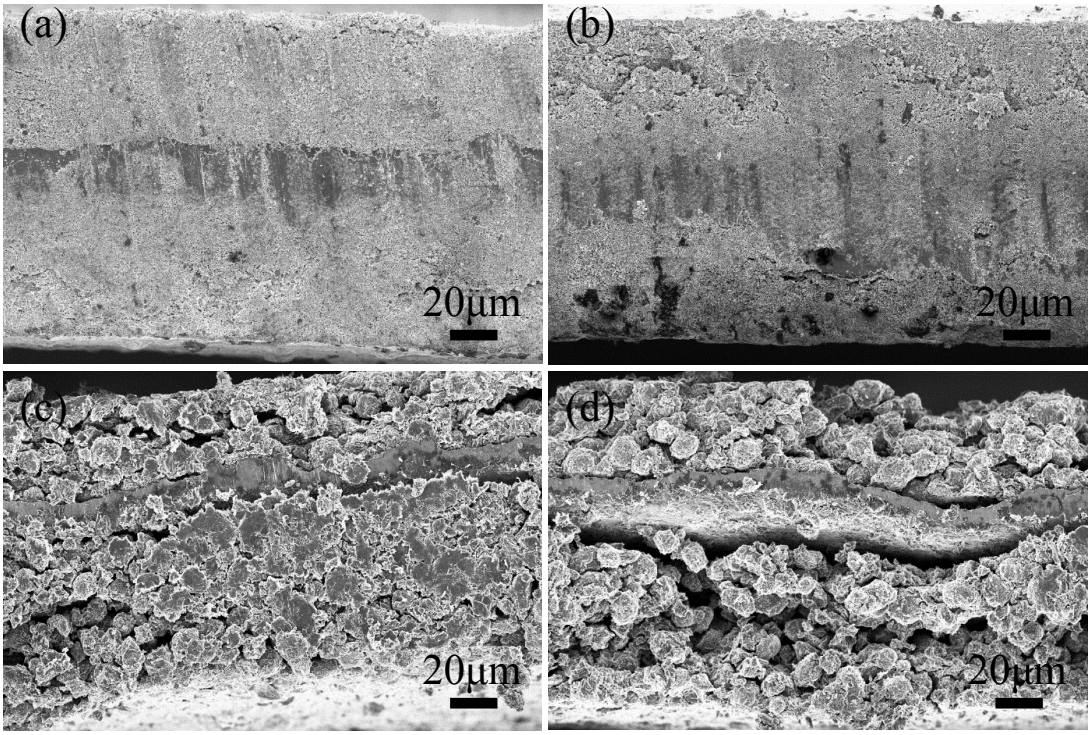

Fig. S17 Cross-sectional SEM images of LFP electrodes (a) healthy (b) unhealthy; and cross-sectional SEM images of graphite electrodes (c) healthy (d) unhealthy.

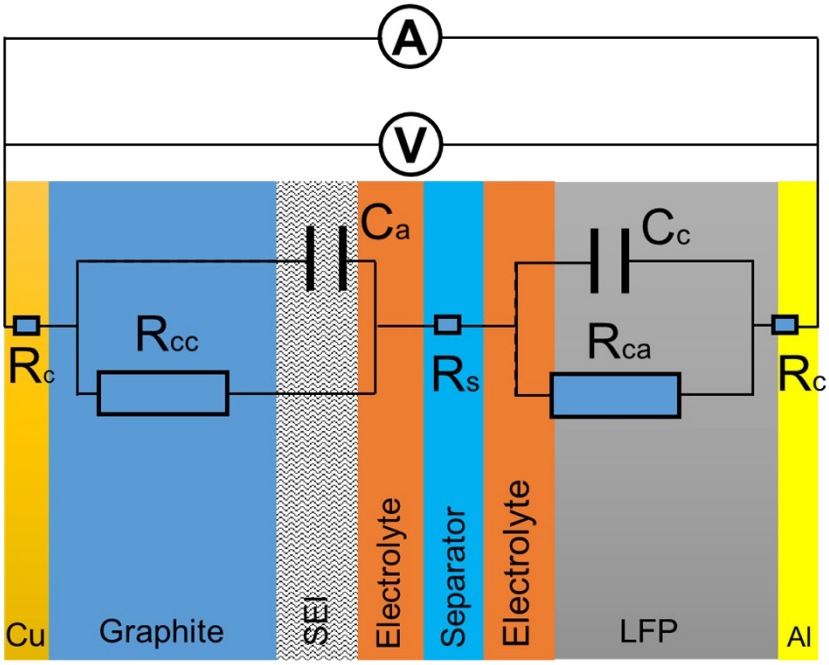

Fig. S18 The full battery model used to generate voltage response under large amplitude constant current step polarization

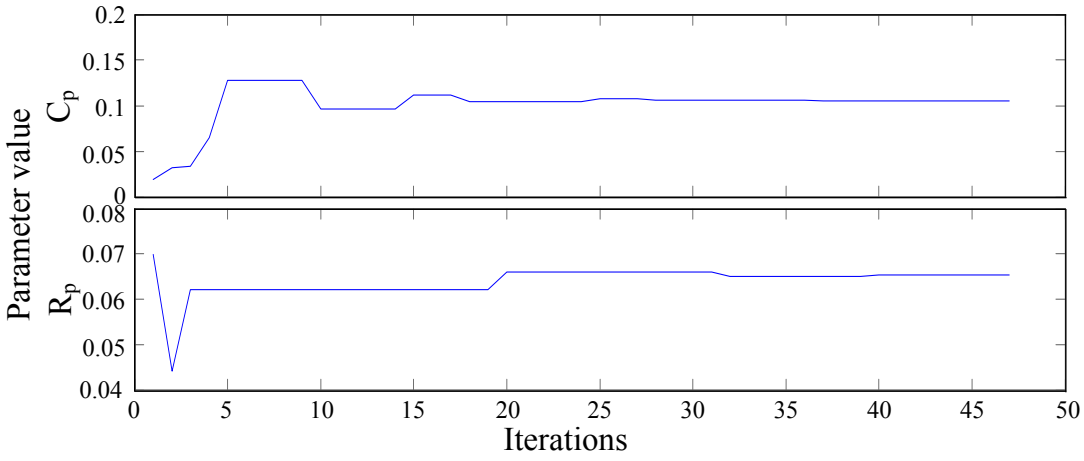

Fig. S19 Trajectories of estimated parameters R_p and C_p

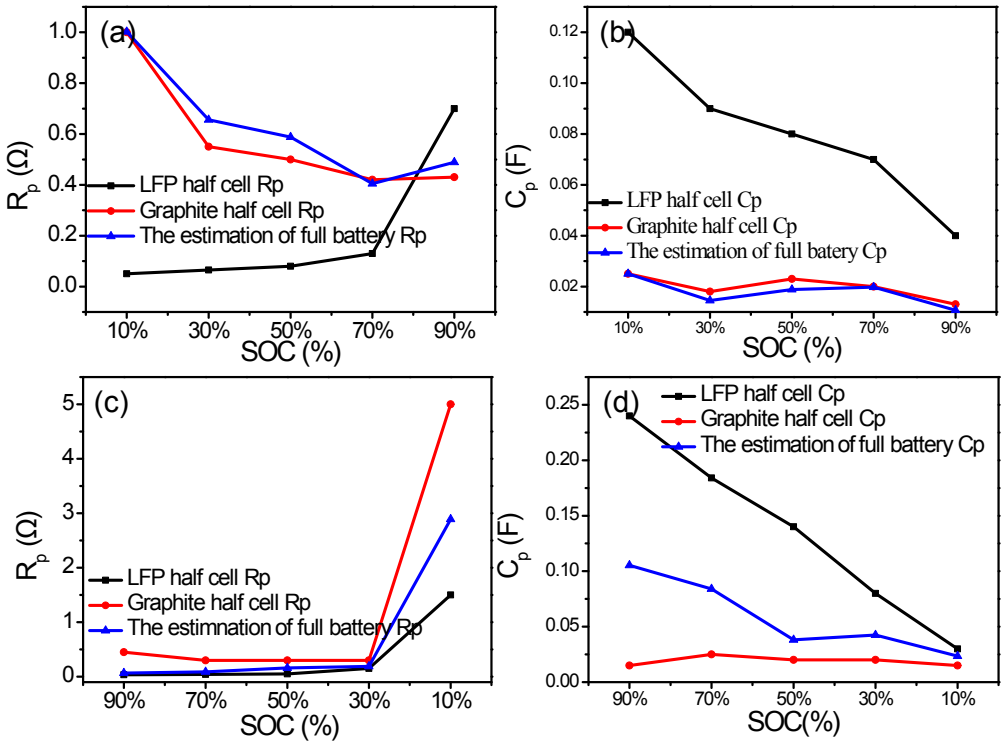

Fig. S20 The R_p relationship of LFP, graphite half-cells and the estimate data of full battery during the (a) charge (c) discharge process, the C_p relationship of LFP, graphite half-cells and the estimate data of full battery during the (b) charge (d) discharge process.

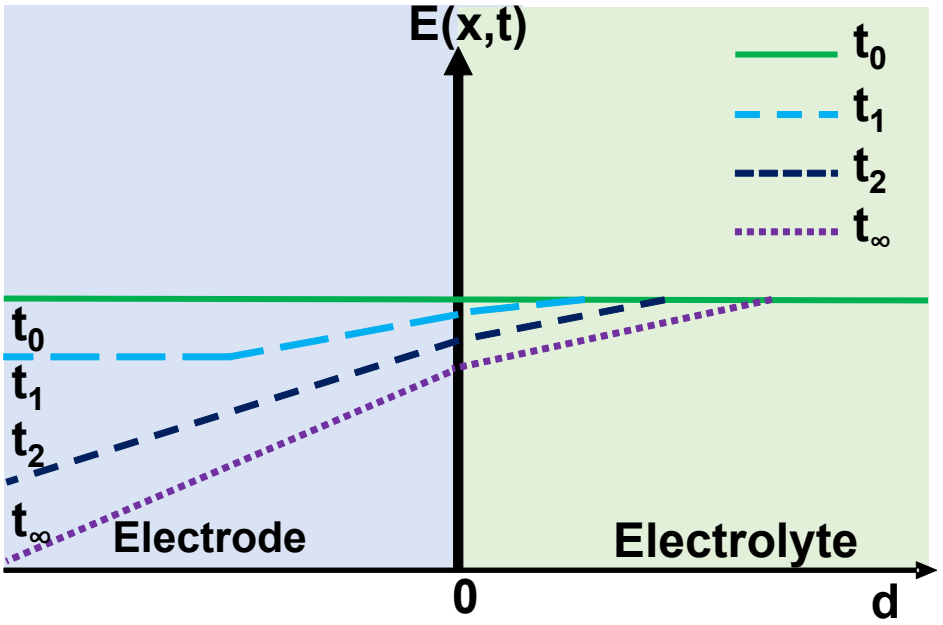

Fig. S21 Diagram of potential distribution curves in electrode and electrolyte: t_0=0; t_1=τ/16; t_2=τ/4; t_3=9/16τ; t_4=τ, τ is transient time.

References

1. Yamada, H.; Moriguchi, I.; Kudo, T. *Journal of Power Sources* **2008,** 175, (1), 651-656.
2. Moriguchi, I. *Chemistry Letters* **2014,** 43, (6), 740-745.
3. Bard, A. J.; Faulkner, L. R.; Bard, A.; Faulkner, L., *Electrochemical Methods: Fundamentals and Applications, 2nd edn*. Wiley*: 2001